



Attention-driven graph convolutional neural networks for mineral prospectivity mapping[☆]



Changjie Cao^a, Xiuliang Wang^{a,*}, Fan Yang^b, Miao Xie^c, Bingli Liu^a, Yunhui Kong^a, Cheng Li^a, Zhongli Zhou^a

^a College Of Mathematics and Physics, Chengdu University of Technology, Chengdu 610059, China

^b College of Computer Science and Cyber Security (Oxford Brookes College), Chengdu University of Technology, Chengdu 610059, China

^c Institute of Geophysical and Geochemical Exploration, Chinese Academy of Geological Sciences, Langfang 065000, China

ARTICLE INFO

Keywords:

Mineral prospectivity mapping
Graph Neural Networks
Attention
Non-Euclidean Space

ABSTRACT

Mineral Prospectivity Mapping (MPM) is a fundamental technique in the field of geosciences for identifying regions with high mineral potential. Graph Neural Networks (GNNs) have been extensively utilized in MPM, particularly excelling in handling non-Euclidean spatial data, effectively addressing the limitation of traditional deep neural networks, which struggle to capture and utilize spatial information. However, they often rely on direct geographic connections, which limit their ability to recognize long-distance geological relationships. This constraint impacts the understanding of mineralization processes and prediction accuracy, while feature smoothing in multi-layer graph convolution operations further weakens the aggregation of distant features. To address these challenges, this study proposes an Attention-Driven Graph Convolutional Network (ADGCN) that leverages an attention mechanism to select highly correlated nodes for connection and aggregates features from distant nodes for representation learning. Building upon the spatial information-capturing capabilities of traditional Graph Neural Networks, ADGCN further optimizes the process by dynamically prioritizing critical nodes, capturing complex spatial patterns and nonlinear relationships while alleviating feature smoothing and enhancing the aggregation of geographically distant but geologically related units. In tests conducted in the Lhasa region, ADGCN achieved an AUC of 91.67%, surpassing GAT by 2.65%, demonstrating superior prediction accuracy in MPM.

1. Introduction

Mineral Prospectivity Mapping (MPM) is a fundamental tool in geosciences, employed to identify and delineate areas with high potential for mineral deposits (Zuo, 2020). This complex process integrates a variety of datasets, including geological, geochemical, geophysical, and remote sensing information, to develop predictive models that guide mineral exploration and resource assessment (Rajesh, 2004). Over time, the MPM paradigm has evolved significantly, transitioning from traditional knowledge-driven methodologies to more sophisticated data-driven and hybrid models (Bonham-Carter, 1994; Carranza, 2008).

Early MPM models predominantly relied on expert knowledge-driven techniques (Agerberg, 1989), where geological interpretations and expert insights were paramount in identifying potential areas for mineral exploration. Techniques such as weights of evidence provided a

practical framework for integrating various prospecting data. However, these approaches have inherent limitations in capturing the complex relationships and patterns that are often associated with mineralization processes (Zuo and Xu, 2023).

The advent of data-driven approaches, characterized by techniques such as random forest (Rodríguez-Galiano et al., 2014), neural networks (Singer, 2021; Singer and Kouda, 1996), and deep auto-encoders (Xie et al., 2023; Xiong et al., 2018), has introduced more advanced methods for analyzing large datasets. These techniques can reveal intricate nonlinear relationships between geological features and mineral deposits. Despite these advancements, traditional raster-based models struggle to capture nuanced spatial correlations among neighboring raster cells, limiting their ability to fully understand the spatial intricacies of mineralization (Talebi et al., 2022).

To overcome these limitations, recent developments in MPM have

[☆] This article is part of a special issue entitled: 'Metallogeny and Exploration of Cu polymetallic deposits' published in Ore Geology Reviews.

* Corresponding author.

E-mail address: xiuliwang_cdut@163.com (X. Wang).

seen a shift towards image-based and graph-based models. Image-based approaches, particularly convolutional neural networks (CNNs) (Li et al., 2020b; Li et al., 2021; Yang et al., 2021), exploit the spatial characteristics of input images to capture patterns related to mineralization. However, CNNs may face challenges in accounting for the spatial anisotropy of mineral deposits due to their fixed patch sizes, which can limit their capacity to fully capture spatial relationships among geological features, particularly in non-Euclidean spaces (Zuo and Caranza, 2023).

In contrast, GNNs have gained attention for their effectiveness in handling non-Euclidean spatial data. Based on the graph Laplacian operator, GNNs are capable of aggregating neighborhood information; nevertheless, they still encounter problems such as over-smoothing, high computational complexity, and fixed neighborhood ranges. To tackle these challenges, researchers have put forward a series of enhancements. For instance, GraphSAGE (Hamilton et al. 2017) enhances model scalability by sampling neighbors and learning trainable aggregation functions. ResGCN (Li et al., 2019) introduces residual and skip connections to effectively alleviate gradient vanishing and excessive feature smoothing. CKGConv (Ma et al., 2024) incorporates continuous convolution kernels, further strengthening the ability to process complex graph-structured data.

GNNs excel in capturing complex, nonlinear spatial relationships among multiple nodes and their connections, making them particularly well-suited for modeling complex geological phenomena such as the spatial distribution of mineral deposits. (Shi et al., 2024; Xu et al., 2023; Xu and Zuo, 2024; Zuo and Xu, 2023). This capability allows GNNs to address some of the limitations inherent in traditional CNN approaches. However, current MPM methods based on GNNs primarily rely on direct geographic connections to construct graph structures (Sihombing et al., 2024). While this approach simplifies the capture of spatial patterns and correlations in geological data, it inherently limits the model's ability to identify more distant relationships between geological features. As a result, these methods may overlook geographically distant units that, despite their spatial separation, exhibit significant correlations in geological features. Given the complex and widely dispersed geological processes involved in mineral deposit formation, neglecting these long-distance relationships could lead to an incomplete understanding of mineralization, thereby reducing prediction accuracy.

To address these challenges, this paper proposes a novel attention-

driven graph convolutional network (ADGCN) method for mineral prospectivity mapping. ADGCN employs an attention mechanism to select nodes with strong correlations for connection, and utilizes graph convolutional networks to aggregate features from distant nodes for representation learning. This approach not only captures intricate spatial patterns and nonlinear relationships but also effectively mitigates the feature smoothing problem inherent in traditional GNNs, thus enhancing the aggregation of geographically distant yet geologically correlated units. The robustness of the proposed method is validated through comparisons of accuracy (ACC), area under curve (AUC), and the anomaly probability map against existing methods.

2. Geological background and dataset

2.1. Geological background

The Lhasa area, located within the eastern Gangdese belt, is situated between the Bangonghu-Nujiang suture and the Indus-Yarlung Zangbo suture (Fig. 1) (Xie et al., 2023). Its geological structure is complex, characterized by intense magmatic activity and favorable metallogenic conditions, with potential for significant copper-molybdenum, copper polymetallic, lead-zinc, and gold deposits.

The Qinghai-Tibet Plateau has undergone a series of significant geological events, including the fragmentation of the Gondwana continent and the subsequent expansion, subduction, closure, and intra-continental orogeny of the Tethys ocean basin. The plateau is divided into four east-west oriented terranes by three primary suture belts—Jinshajiang, Bangonghu-Nujiang, and Indus-Yarlung Zangbo: namely the Songpan-Ganzi, Qiangtang, Lhasa, and Himalaya terranes from north to south (Pan et al., 2012, Pan et al., 2004). The study area is influenced by dual subduction from both the Meso-Tethys ocean to the south and Neo-Tethys ocean to the north which has resulted in a series of near east-west striking thrust nappe structural systems. This tectonic activity has led to numerous inverted folds and thrust fault zones within the structural belt (Wang et al., 2021).

The study area is geologically divided into the Lhasa-Waka stratigraphic area to the south and the Quesang-Songduo stratigraphic area to the north. In the northern region of Pangduo-Menba, there are exposures of Middle Carboniferous to Early Permian Laigu Formations and Middle Permian Luobadui Formation, characterized by dolomite limestone

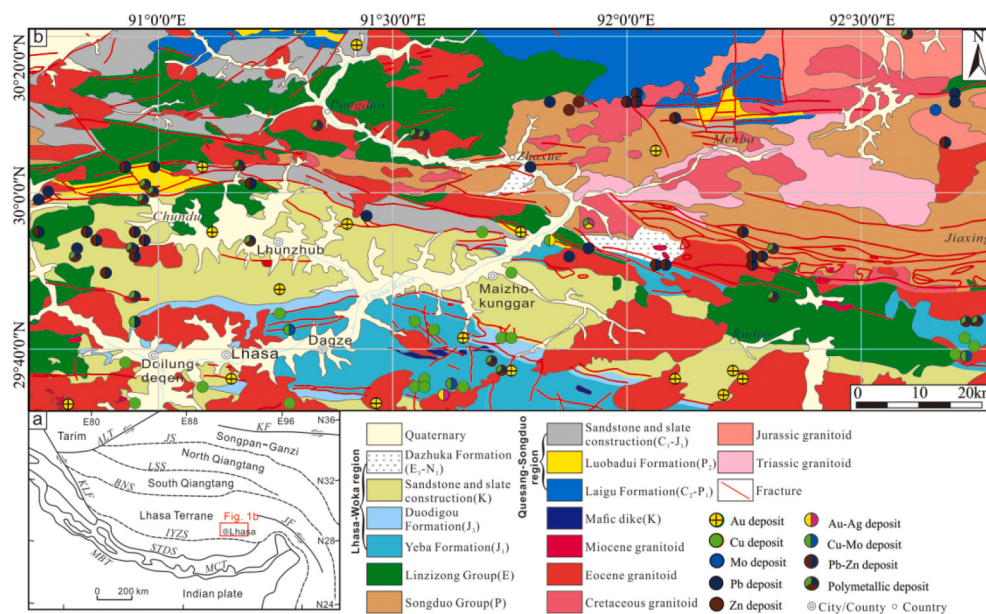


Fig. 1. The Geological background of Lhasa area. (Xie et al., 2023) (a) Geotectonic location of Lhasa area, Tibet. (b) Comprehensive geology and deposit distribution map of Lhasa area, Tibet.

lithology. Conversely, in the southern region, there are formations such as Jurassic Yebadui Formation and Duodigou Formation, consisting of limestone and volcanic clastic rocks.

The region is characterized by extensive intrusive rocks, predominantly granitoids, concentrated within the Gangdese-Nyainqntanglha tectonic magmatic belt. These granites are primarily categorized as I-type granites. Furthermore, Cretaceous-Paleogene granites are widely distributed, particularly in the south-central portion of the Gangdese metallogenic belt, contributing to the formation of the Gangdese batholith (Wang et al., 2014). Miocene granites are commonly associated with porphyry copper deposits intruding into strata, alongside Cretaceous-Paleogene granites (Tang et al., 2015).

The region encompasses four primary deposit types: porphyry, porphyry-skarn, hydrothermal vein, and skarn. Qulong (Tang et al., 2012) is distinguished as a significant porphyry deposit rich in copper and molybdenum, characterized by porphyry-skarn mineralization and influenced by intermediate-acid rock mass, with Jiama serving as a typical example. Skarn deposits, such as Dongzhongla Cu-Zn-Pb-Ag, are primarily associated with magmatic activity, while hydrothermal vein deposits like Riwuduo may be closely linked to regional Miocene porphyry intrusion. During the Paleogene period, the collision between the India-Asia continents initiated intense volcanic-magmatic processes in the Gangdese belt, resulting in significant mineralization (Ji et al., 2012; Xuan-Xue et al., 2005). This led to the formation of several mineral concentrated areas, including the Dongzhongla-Yaguila skarn Pb-Zn and porphyry Mo concentrated area, the Mengyaa-Longmala-Hahaigang skarn Pb-Zn-W-Mo concentrated area, the Lietinggang-Leqingla skarn Pb-Zn-Fe-Cu concentrated area, and the Xingaguo-Lunlang skarn Pb-Zn concentrated area around the Lhunzhub Basin. During the Miocene, as the India-Asia plate entered the post-collisional period, slab breakoff or regional extension of the Neo-Tethys oceanic crust led to mantle material upwelling, initiating Gangdese porphyry and skarn Cu-Mo mineralization (Hou et al., 2006). This process resulted in the formation of the Qulong-Jiama porphyry-skarn Cu-Mo concentrated area. Simultaneously, the India-Asia continental collision transitioned into the “soft collision” stage (Xu et al., 2021), leading to the formation of hydrothermal vein Pb-Zn and Au mineral concentrated areas, such as Riwuduo-Banduoxi Pb-Zn-Ag and Nongruri Au mineral concentrated areas in the study area (Li et al., 2020a).

2.2. DataSet

The geochemical data for the study area were obtained from the Regional Geochemistry National Reconnaissance (RGNR) program (Xie et al., 2008; Xuejing et al., 1997). Stream sediments were chosen as the

sampling medium, with a sampling density of 1 sample per 25 km^2 in the northern part of the region and 1 sample per 4 km^2 in the southern part. Each sample was analyzed for a total of 39 elements. The study area was systematically divided into 6000 prediction units using a grid-based system. Fig. 2 depicts the spatial distribution of Cu elements across the study area.

3. Methodology

The proposed methodology for Mineral Prospectivity Mapping (MPM) is based on an Attention-Driven Graph Convolutional Network (ADGCN) framework (Fig. 3). This framework integrates compositional data analysis with advanced graph neural network techniques to effectively capture complex spatial relationships among geological features.

3.1. Graph neural networks

Graph Neural Networks (GNNs) are a category of deep learning models specifically tailored for processing graph-structured data, which consists of nodes representing data objects and edges representing the relationships between nodes (Wu et al., 2020; Zhou et al., 2020). This makes GNNs well-suited for tasks involving complex dependencies in non-Euclidean spaces. Traditional machine learning and deep learning methods, which primarily handle tabular and image data, are not directly applicable to graph data due to its inherent structure. GNNs address this limitation by utilizing graph convolutional operations to aggregate information from a node's neighbors, thereby enabling the model to learn from the topological structure of the graph and make predictions (Kipf and Welling, 2016).

The fundamental process of GNNs consists of several crucial stages (Scarselli et al., 2008). Initially, graph data is organized into nodes and edges, with each node potentially containing multiple attributes and the edges representing specific relationships or connections between nodes. The nature of these connections is determined based on the user's domain-specific requirements. Once the data is prepared, the GNN proceeds with message passing, where each node transmits its attribute information to its immediate neighbors. This step allows nodes to iteratively gather information from their surroundings, enabling the model to capture the relationships between them. Following message passing, an aggregation step takes place in which each node combines the received information using operations such as summation, averaging, or taking the maximum. These aggregation operations must adhere to permutation invariance by not depending on the order in which neighboring nodes are processed.

After aggregating messages, the node's attributes are updated by integrating its initial features with the aggregated messages using a

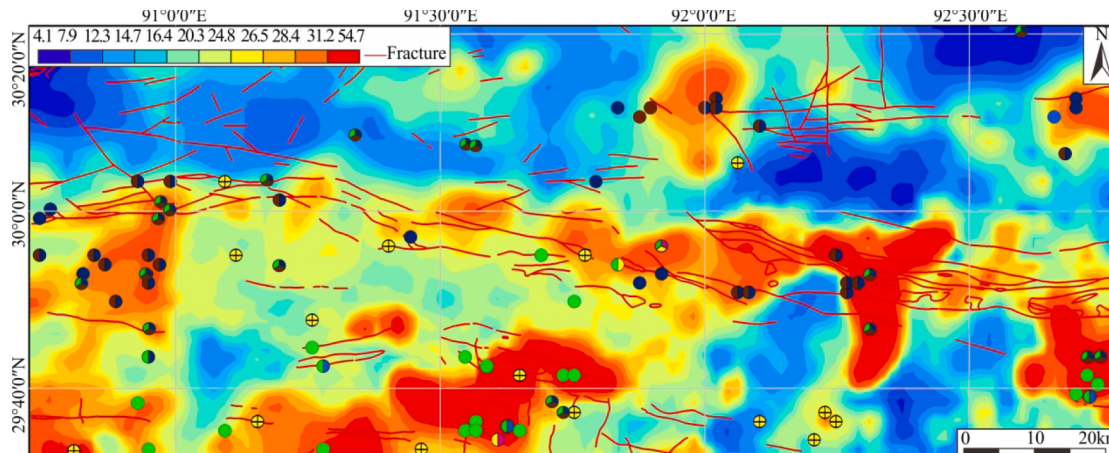


Fig. 2. The spatial distribution of Cu elements across the study area.

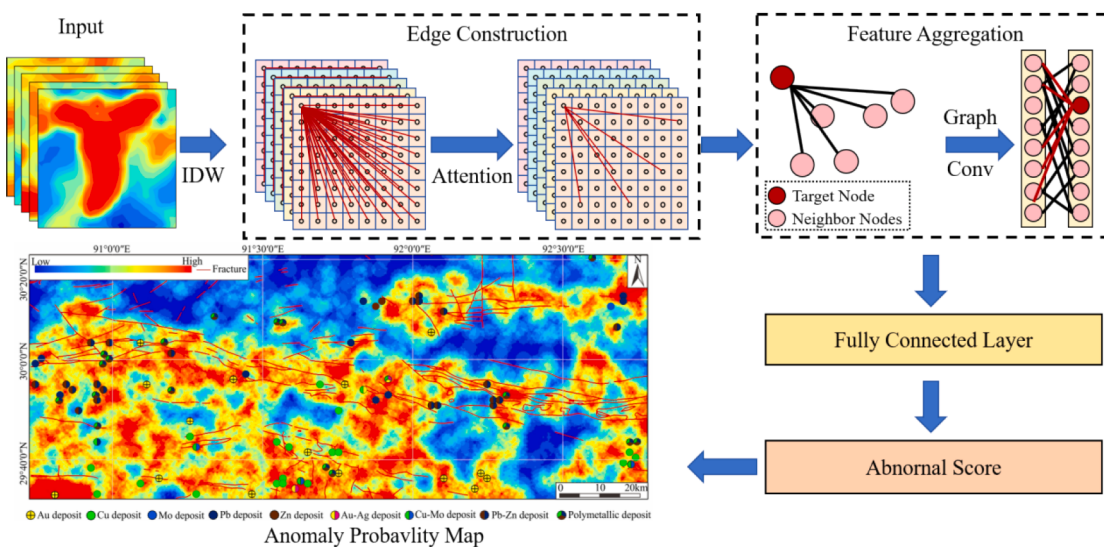


Fig. 3. The Network Structure Diagram of ADGCN: ADGCN integrates an attention mechanism to selectively aggregate information from relevant nodes.

trainable function that includes learnable weights and biases. This process is repeated for multiple layers, with each GNN layer propagating information further across the graph. The depth of the GNN determines how much information is transmitted from distant nodes within the network. After multiple layers of message passing, the final node representations are utilized for tasks such as node classification or regression. The goal of GNN training is to minimize prediction error, typically through a loss function like cross-entropy. Using backpropagation, the model iteratively adjusts its weights to optimize the node representations so that nodes with the same label are as similar as possible, while those with different labels are more distinct.

One commonly utilized variant of GNNs is the Graph Convolutional Network (GCN) (Kipf and Welling, 2016), which updates node information through the aggregation of features from neighboring nodes using a weighted sum, where the weights are dependent on the degree of connection between nodes. Another widely employed variant is the Graph Attention Network (GAT) (Veličković et al., 2017), which improves upon GCNs by integrating an attention mechanism to discern the significance of different neighboring nodes. In contrast to GCNs, which treat all neighbors equally based on node degree, GAT assigns distinct attention weights to each neighbor, enabling the model to prioritize the most relevant nodes when aggregating information. This is accomplished through an attention mechanism that computes attention coefficients based on connected node features, providing greater flexibility for capturing intricate relationships within the graph.

While both GCN and GAT have achieved considerable success in various graph-based tasks, they exhibit certain limitations when employed in MPM. The dependence of GCN on aggregating information from neighboring nodes through a weighted sum based on node degree can lead to the over-smoothing problem, where the features of distant nodes are diluted after multiple layers of convolution. This causes the loss of crucial spatial and geological details, especially in regions where long-range geological relationships are significant. Conversely, GAT makes an improvement on GCN by incorporating an attention mechanism to prioritize more relevant neighbors. However, its focus is still mainly on local, geographically adjacent nodes, limiting its ability to capture long-distance geological correlations that are often essential for mineral exploration. These deficiencies can hinder the model's capacity to effectively represent complex geological patterns, thereby leading to poor performance in mineral prospectivity mapping.

This study adopts a hybrid approach that integrates an attention mechanism for edge construction with GCNs for node feature aggregation and prediction. Specifically, the attention mechanism is employed

to assign weights to the edges in the graph, eliminating those edges with low attention coefficients to establish an optimized graph structure. Subsequently, GCN is employed on this graph to aggregate information from neighboring nodes and update node representations. This fusion of attention-driven edge construction and GCN-based feature aggregation effectively strengthens the connection between geographically distant but geologically related units, thereby significantly enhancing the accuracy of the model in label prediction tasks.

3.2. Graph construction

The graph construction process is pivotal in the methodology as it facilitates the modeling of spatial relationships among geological features using graph theory principles. Let $G = (V, E)$ denote the graph, where V represents the set of nodes (rasters) and E denotes the set of edges connecting these nodes. The connections are established in accordance with the spatial relationships among the grids, and the attention coefficient is computed to gauge the significance of the connections. Through iterative updates, the attention mechanism dynamically modulates the weights of the edges, reinforcing key spatial dependencies while attenuating weaker or irrelevant connections. Eventually, the resultant graph can effectively represent the spatial relationships among the grids.

3.2.1. Node representation

Each raster i in the Mineral Prospectivity Mapping dataset corresponds to a node v_i within the graph G . The feature vector denoted as h_i is associated with node v_i , encompassing geochemical properties.

3.2.2. Edge construction

The objective of this step lies in constructing the edges of a graph, which can effectively capture the significant spatial relationships between rasters by means of a learnable attention mechanism from graph attention networks. Through iterative updates, the attention mechanism dynamically modulates edge weights, reinforcing important spatial dependencies while attenuating weaker or irrelevant connections. This adaptive process guarantees that the most significant relationships between nodes are retained, enabling the graph to precisely reflect the underlying spatial structure of the rasters.

The process is illustrated in Fig. 4. Initially, all rasters in the image are connected to form a unified graph structure. Each raster i in the MPM dataset is represented as a node v_i in the graph G , ensuring inter-connectivity among all rasters.

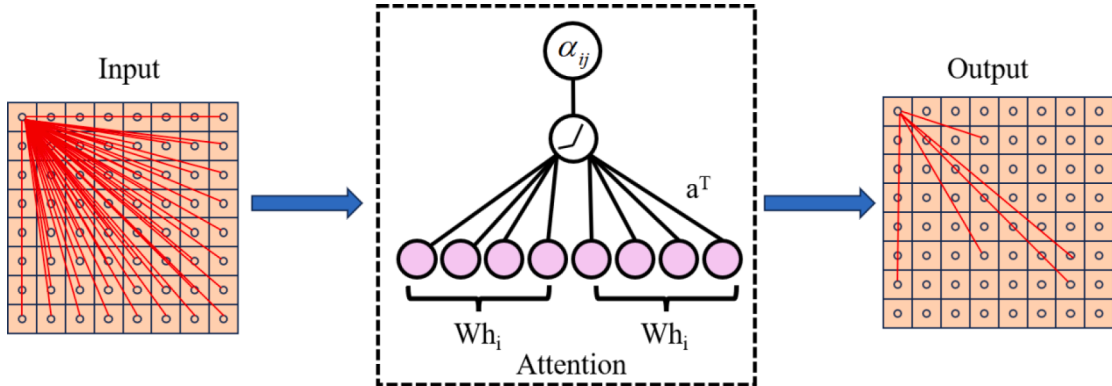


Fig. 4. The process of edge construction.

The attention score α_{ij} between nodes i and j in the graph is computed based on their features using a learnable attention mechanism. Let h_i and h_j denote the feature vectors of nodes i and j , respectively. The attention score α_{ij} is calculated as:

$$\alpha_{ij} = \text{LeakyReLU}(a^T [Wh_i || Wh_j])$$

where a is a learnable attention parameter vector, W is the weight matrix, \parallel denotes concatenation, and LeakyReLU is the leaky rectified linear unit activation function.

After computing the attention scores, the top five edges with the highest attention coefficients are retained for each raster. This approach ensures that the most significant connections are maintained while maintaining consistency across different datasets and scenarios. By selecting a fixed number of edges, the computational process is simplified, the variability of the graph structure is reduced, and stability during graph training is ensured.

These edges signify crucial spatial relationships between grids, as determined by attention mechanisms. By initially establishing connections between all rasters and selecting edges with high attention coefficients, the model prioritizes connections that contribute most to spatial patterns and correlations in the MPM dataset. This selective edge formation process effectively enhances the model's capacity to capture important geological features and improves accuracy in MPM.

3.3. Feature aggregation

Following the formation of the graph structure and the calculation of attention coefficients, the graph convolution operation is performed to aggregate information from neighboring nodes and update the feature representations of each node. The process is illustrated in Fig. 5.

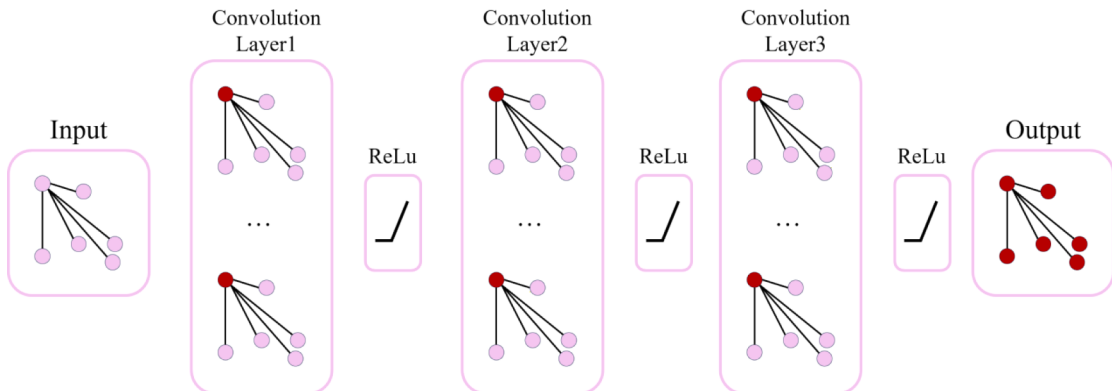


Fig. 5. The process of feature aggregation.

3.4. Loss function

To train the proposed model for mineral prospectivity mapping (MPM), the cross-entropy loss function is utilized to measure the discrepancy between the predicted probability distribution and the true labels of the mineral deposits. Let \hat{y}_i denote the predicted probability of raster i belonging to a mineral deposit class, and let y_i denote the ground truth label indicating the presence or absence of mineral deposits. The cross-entropy loss L is calculated as:

$$L = -\frac{1}{N} \sum_{i=1}^N (y_i \log(\hat{y}_i) + (1 - y_i) \log(1 - \hat{y}_i))$$

where N is the total number of rasters in the dataset.

The cross-entropy loss function (Rubinstein, 1999) penalizes the model for deviations between the predicted probabilities and the ground truth labels, encouraging the model to learn accurate representations of mineral prospectivity. By minimizing the cross-entropy loss during training, the model optimizes its parameters to better predict the presence of mineral deposits, thereby improving the effectiveness of mineral prospectivity assessments.

4. Results and discussion

4.1. Experimental setup

In this study, the Inverse Distance Weighted (IDW) (Shepard, 1968) interpolation method was employed to convert relevant data into raster format, which served as input for all models. The selection of samples involved primarily using negative samples from low-potential regions located far from mineralization points and outside fault buffer zones, ensuring an even and random distribution across the study area. Conversely, due to the rarity of mineralization events, positive samples were confined to the mineralized zones.

The dataset consists of 117 positive samples and 123 negative samples, each sized 28×28 . Data augmentation techniques were employed to expand the dataset and ensure an adequate number of positive and negative samples. Specifically, 25 distinct sub-patches of size 24×24 were generated for each patch without overlap, thereby maximizing the size of the training samples. As a result, a total of 2925 positive samples and 3075 negative samples were obtained. Additionally, 80 % of the samples were randomly selected for training, while the remaining 20 % were designated for testing. Each node in the graph neural network solely utilizes information from 39 geochemical elements.

The GCN and GAT models are composed of 4 graph convolutional layers or 4 attention layers, respectively. Except for the last layer, ReLU activation functions are applied to all layers. To prevent overfitting, a dropout layer with a dropout rate of 0.125 for GCN and 0.175 for GAT is added before each layer. Finally, log softmax is used for classification. During training, the Adam optimizer is utilized to minimize the loss. For the GNN models, the number of iterations is set to 100, and the learning rate is set to 0.001.

ADGCN commences with a graph attention layer, which ascertains the significance of connections among nodes. Based on the attention scores, all edges related to the top 7 nodes are chosen as inputs for the subsequent 3 GCN layers. These GCN layers further enhance the

extracted features. Eventually, classification is carried out through a linear layer. During training, the Adam optimizer is employed to minimize the loss function, with the number of iterations set at 100 and the learning rate fixed at 0.001. The specific model parameters are detailed in Table 1.

4.2. Ablation study

To obtain the best performance in terms of AUC and ACC, an ablation study was carried out to determine the ideal number of top nodes based on attention scores. During the testing stage, the model utilized an attention mechanism to identify the most significant edges. From the points connected by these edges, the top-k nodes with the highest connection frequencies were chosen. These nodes then served as the basis for determining whether a sample presented anomalous mineralization. The study evaluated the model's performance by varying the selection of top nodes from 1 to 30 and measuring the corresponding AUC and ACC values.

The results, illustrated in Fig. 6 and Fig. 7, indicate that the ADGCN model reaches the highest AUC and ACC when selecting the top 7 nodes. This demonstrates that choosing the top 7 nodes provides the most effective configuration for the model, optimizing both the AUC and ACC metrics simultaneously.

Selecting fewer than 7 nodes resulted in decreased AUC and ACC values, indicating that a smaller subset of nodes may not capture sufficient critical information for accurate predictions. Conversely, selecting more than 7 nodes did not lead to a significant improvement in performance and, in some cases, even resulted in a decrease in AUC. This suggests that adding additional nodes beyond the top 7 does not substantially enhance model performance and may introduce unnecessary complexity.

The ablation study overall confirms that the optimal number of top nodes for achieving the best AUC and ACC in the ADGCN model is 7, emphasizing the importance of selecting a balanced number of influential nodes to ensure optimal performance in mineral prospectivity mapping.

4.3. Comparative experiment with GCN and GAT

A comparative experiment is conducted to assess the performance of the ADGCN model in comparison to two other graph neural network models, namely GCN and GAT. The performance metrics under consideration include Accuracy (ACC) and Area Under the Curve (AUC).

Table 2 illustrates the Accuracy values for ADGCN, GCN, and GAT. The findings reveal that ADGCN achieves the highest Accuracy of 83.55 %, outperforming GCN's 81.89 % and GAT's 82.02 %. This highlights the superior predictive capability of ADGCN in accurately assessing mineral prospectivity.

Fig. 8 shows the AUC values for ADGCN, GCN, and GAT. The results reveal that ADGCN has the highest AUC of 91.67 %, exceeding GCN's 87.90 % and GAT's 89.02 %. This highlights ADGCN's superior ability to discriminate between positive and negative classes across various thresholds.

These findings underscore the effectiveness of the ADGCN model in mineral prospectivity mapping, demonstrating its ability to provide

Table 1

Detailed parameter configurations of GCN, GAT, and ADGCN models.

Model		GNN Layer1	GNN Layer2	GNN Layer3	GNN Layer4	Linear1	Linear2
GCN	input	39	64	128	64	576*32	64
	output	64	128	64	32	64	2
GAT	input	39	64	128	128	576*32	64
	output	64	128	128	32	64	2
ADGCN	input	39	64	128	–	576*32	64
	output	64	128	32	–	64	2

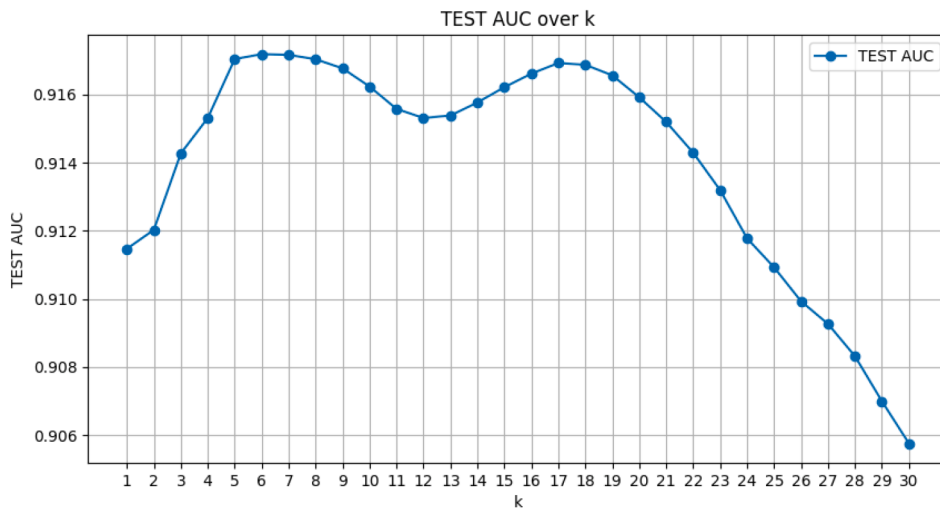


Fig. 6. AUC of ADGCN with different values of k: The network achieves the highest AUC when k = 7.

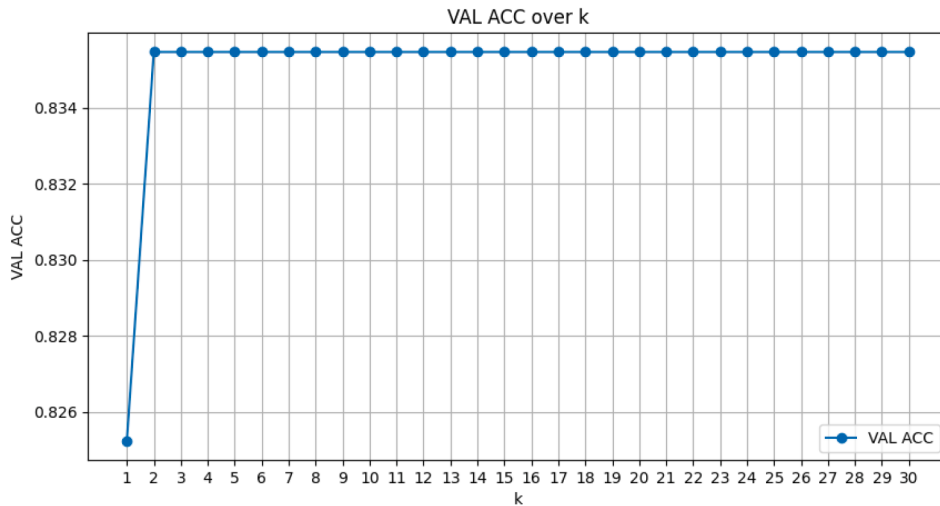


Fig. 7. ACC of ADGCN with different values of k: The ACC remains unchanged after k = 2.

Table 2
Accuracy Comparison of ADGCN, GCN, and GAT.

Model	Accuracy
ADGCN	83.55 %
GCN	81.89 %
GAT	82.02 %

more accurate and reliable predictions compared to traditional GCN and GAT models. However, there is still scope for improvement, especially when it comes to addressing potential challenges like the quality of the constructed graph structure. Future endeavors might concentrate on refining graph construction by means of enhanced preprocessing techniques and the integration of geological knowledge to further enhance model performance.

4.4. Visualization experiment

The visualization of the top 7 nodes with the highest attention scores from the ADGCN model effectively highlights regions with significant mineral prospectivity.

Fig. 9(a) presents the distribution of the first seven key nodes in the non-Euclidean spatial graph structure, thereby uncovering the significant spatial relationships and connection patterns identified by the model in mineral prospect prediction. Fig. 9(b) maps these key nodes onto the geographic grid of Euclidean space to present their specific geographic locations. These high-ranking nodes exhibit obvious aggregation patterns in specific regions, which implies that these regions can precisely reflect the metallogenic probability of the area and can accurately identify the regions with greater mineral resource potential, thereby enhancing the predictive capacity of the model in mineral exploration.

This clustering pattern not only validates the predictive accuracy of the model but also demonstrates its interpretability. The attention mechanism reveals the most influential nodes, providing insights into

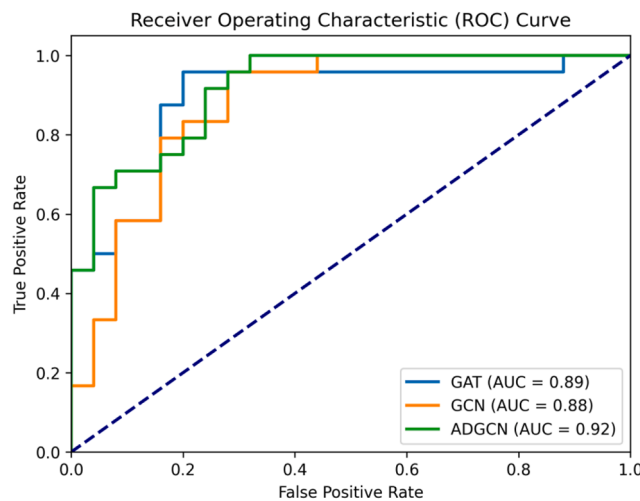


Fig. 8. AUC Comparison for ADGCN, GCN, and GAT: ADGCN achieves the highest AUC.

the underlying spatial relationships that drive the predictions. By illustrating how the model prioritizes certain nodes, the visualization helps to understand the rationale behind mineral prospectivity assessments, confirming that the ADGCN model effectively highlights key areas of interest.

The visualization confirms the effectiveness and interpretability of the ADGCN model. The attention mechanism's ability to cluster key nodes in regions of known mineralization potential is consistent with existing geological knowledge, providing a reliable and comprehensible framework for assessing mineral prospectivity.

4.5. Mineral prospectivity mapping

In the MPM prediction experiments, three distinct prospectivity maps were generated using the GCN, GAT, and ADGCN models. Each map visualizes the predicted mineral prospectivity across the study area, with varying levels of detail and accuracy as determined by each model. Fig. 10, Fig. 11, and Fig. 12 present the mineral prospectivity maps produced by GCN, GAT, and ADGCN, respectively.

The prospectivity map generated by the GCN model (Fig. 10) shows a relatively uniform distribution of prospectivity scores, with limited differentiation between high- and low-potential areas. This is mainly attributed to the inherent limitations of the GCN model, especially its reliance on aggregating information from neighboring nodes through a weighted sum based on node degree. This approach often causes the over-smoothing problem, where the features of distant nodes are diluted and lose their distinctiveness after multiple layers of convolution. Consequently, the model has difficulty in effectively capturing the key metallogenetic factors and favorable mineralization conditions that are crucial for influencing mineral deposit formation. The resulting uniformity in prospectivity scores may mask important areas of interest.

The GAT map (Fig. 11) effectively distinguishes areas with higher and lower prospectivity, demonstrating the model's attention mechanism that allows for precise identification of key geochemical anomaly zones. However, this success mainly stems from the model's focus on neighboring nodes based on the attention mechanism. Although GAT assigns different weights to neighboring nodes, its attention is still mainly concentrated on local, geographically adjacent nodes, restricting its ability to capture long-distance geological relationships. This limitation restricts the model's capacity to fully represent more dispersed geological features. As a result, while the GAT model does identify regions of interest, it might overlook potential mineralization in areas that are geographically distant but still show significant geological

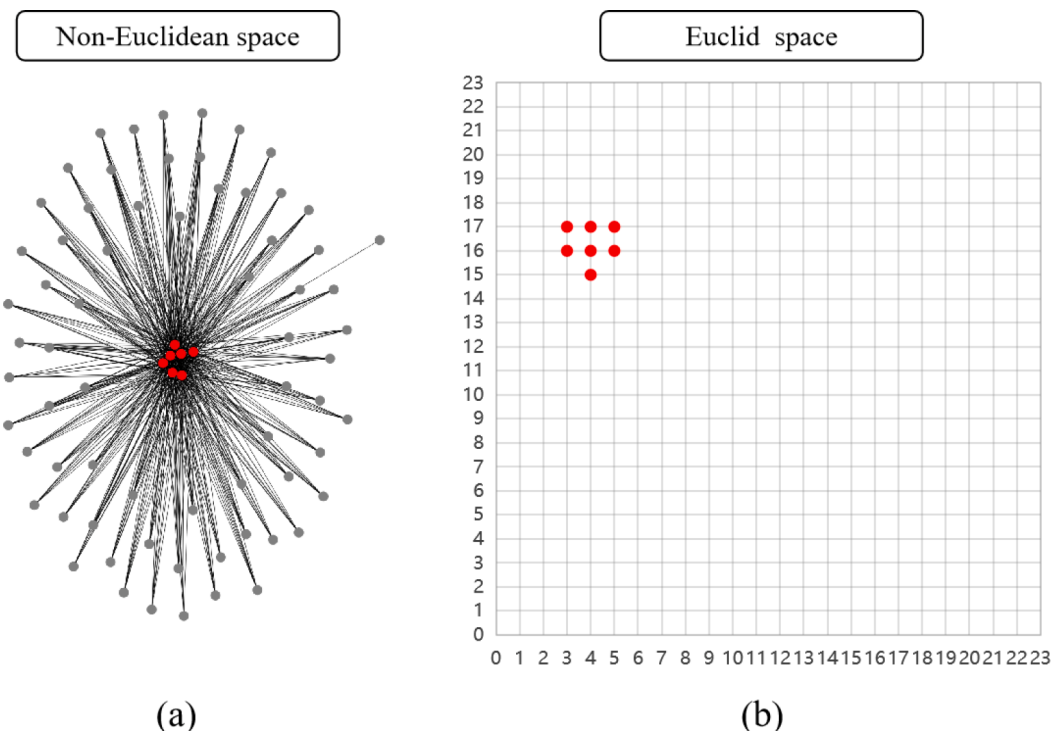


Fig. 9. The visualization of the top 7 nodes. (a) Positions of top-ranked nodes within the non-Euclidean graph structure.(b) Specific locations of the top-ranked nodes within the Euclidean spatial grid.

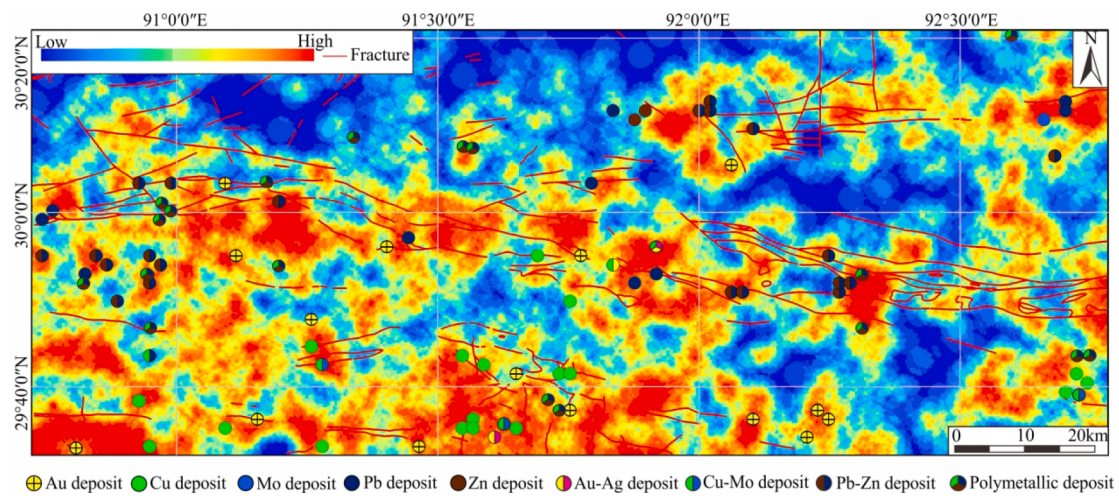


Fig. 10. The visualization of the mineral prospectivity map using GCN.

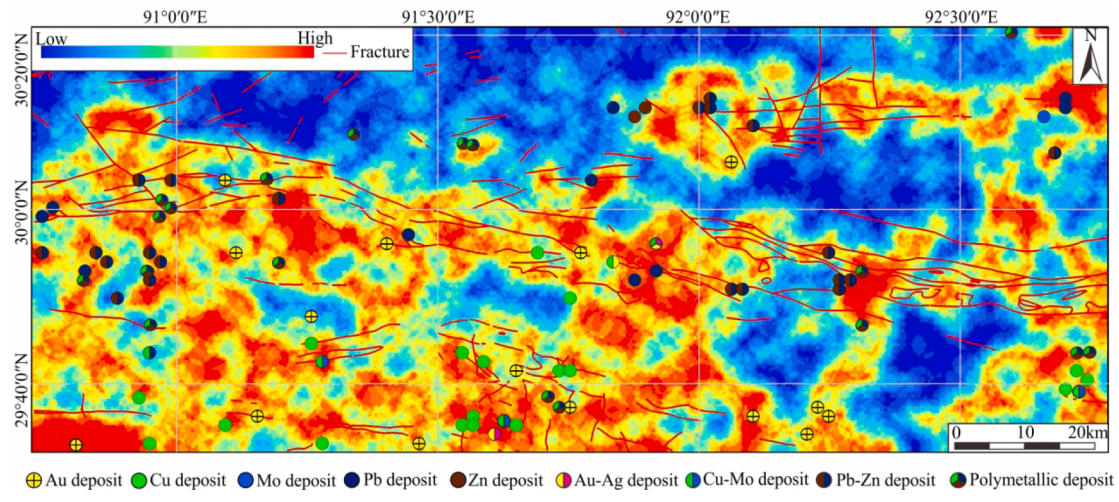


Fig. 11. The visualization of the mineral prospectivity map using GAT.

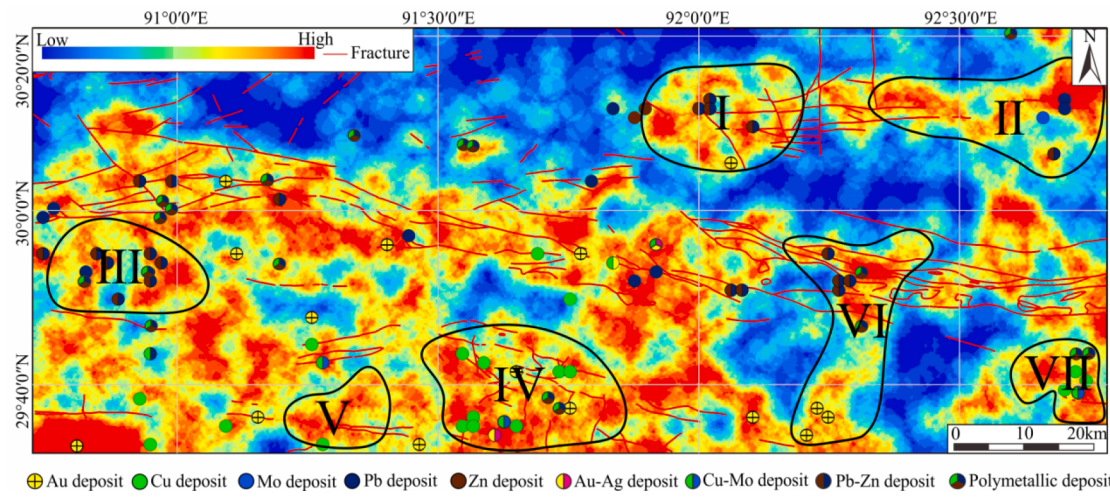


Fig. 12. The visualization of the mineral prospectivity map using ADGCN.

correlations, which could be crucial for a more comprehensive mineral prospectivity map.

The ADGCN map (Fig. 12) demonstrates superior ability in precisely

delineating critical mineralization zones, thanks to its advanced edge construction techniques and convolutional operations. The model is outstanding in capturing geological features associated with high

mineralization potential. For example, the model effectively delineates regions where silicification, chloritization, and other alteration types exist, which are typically associated with skarn Pb-Zn and porphyry-skarn Cu deposits. The strong correlation between the ADGCN predictions and known hydrothermal alteration zones or mineralized bodies verifies the model's effectiveness in identifying high-potential areas.

In summary, the comparative analysis of the three models highlights the advantages of the ADGCN model in generating detailed mineral prospectivity maps. The ADGCN model leverages geochemical background information to learn spatial information from the distribution of chemical element data, thereby identifying favorable metallogenic conditions. This approach deepens the understanding of metallogenic processes and provides valuable guidance for future mineral exploration activities in the study area.

Target I is situated in the northern area of the Nyainqntanglha metallogenic belt, where granite porphyry is the predominant exposed rock, closely associated with Pb and Zn element (Wang et al., 2015). The mineral bodies in this potential area exhibit layered and veined structures along fractures, accompanied by the development of typical skarn minerals. This highlights ADGCN's ability to effectively capture spatial information and identify favorable mineralization conditions, demonstrating its strength in modeling complex geological relationships and pinpointing areas with significant prospectivity potential.

Target II is situated in the northeastern part of the Lhasa area, a key polymetallic ore concentration zone within the northern Gangdese belt. This region shows prominent anomalies of Mo, Pb, Ag, and Zn, with the Luobadui and Laigu Formations being favorable metallogenic strata. The Late Yanshanian-Early Himalayan intermediate-acidic magmatism enriched essential metallogenic elements along fractures, providing favorable conditions for mineralization. By using only geochemical data, the ADGCN model effectively captures crucial spatial information, demonstrating its ability to integrate and identify mineralization-related anomalies. This highlights the model's capability to accurately detect areas with considerable exploration potential.

Target III is located in the northern section of central Gangdese, a region marked by well-developed fractures, folds, and frequent magmatic activities, along with significant alterations of the wall rock, such as skarnization, silicification, and carbonation. These geological characteristics provide an ideal environment for skarn Pb-Zn deposits. This validates the ADGCN model's outstanding ability to capture both local geological features and distant spatial relationships. By leveraging its attention mechanism, the model effectively acquires critical metallogenic factors, further highlighting its potential in mineral prospectivity analysis.

Target IV is located in the southern part of the study area, characterized by NW-SE trending ore-controlling fractures, complemented by secondary fractures in NE-SW, nearly NS, and nearly EW directions. The complex tectonic processes in this region are closely related to mineralization, as indicated by metallogenic geochemical associations showing significant metal enrichment. This demonstrates the strong identification capabilities of the ADGCN model, which is outstanding in effectively highlighting areas with high mineralization potential.

Target V is west of Target IV, where intermediate-acid intrusive veins like granodiorite porphyry and quartz monzonite porphyry suggest multiple magmatic events closely related to mineralization. The clear mineralization around veins, along with favorable metallogenic rocks and high ADGCN prediction values, indicate further exploration potential.

Target VI is located in the southeast corner of the study area. Strong tectonic activity and compressional orogeny create favorable conditions for ore-bearing hydrothermal fluid migration ADGCN predictions highlight significant metallogenic potential, suggesting this as a promising area for porphyry-skarn Cu deposits.

Target VII is a primary zone for hydrothermal vein Pb-Zn/Au deposits. The metallogenic element anomalies, controlled by fractures and

rock masses, display a wide range of values exceeding the background level. This indicates exploration potential for orogenic gold deposits in addition to Pb-Zn mineralization.

5. Conclusion

This study presents a novel ADGC: Attention-Driven Graph Convolutional Network for Mineral Prospectivity Mapping, which enhances the prediction accuracy and interpretability of mineral deposit assessments. The proposed method effectively integrates an attention mechanism with graph convolutional operations to capture complex spatial relationships and nonlinear dependencies among geological features. The experimental results demonstrate that ADGCN outperforms traditional Graph Convolutional Networks and Graph Attention Networks in terms of Accuracy and Area Under the Curve. Specifically, ADGCN achieves the highest ACC of 83.55 % and AUC of 91.67 %, highlighting its superior performance. The ablation study confirms that selecting the top 7 nodes provides optimal results, balancing model complexity and performance. Visualization experiments further validate the interpretability of ADGCN by effectively identifying key areas with high mineral prospectivity, consistent with geological knowledge.

Declaration of competing interest

The authors declare that they have no known competing financial interests or personal relationships that could have appeared to influence the work reported in this paper.

Acknowledgments

This work was supported by the Natural Science Foundation of Sichuan under Grant 2023NSFSC1422, the National Key R&D Program of China (Grants 2022YFC2905002), the National Natural Science Foundation of China (42072322), and the Sichuan Science and Technology Program (2023NSFSC0277).

Data availability

The authors do not have permission to share data.

References

- Agterberg, F.P., 1989. Computer programs for mineral exploration. *Science* 245, 76–81.
- Bonham-Carter, G., 1994. *Geographic Information Systems For Geoscientists: Modelling With GIS*. Elsevier.
- Carranza, E.J.M., 2008. *Geochemical Anomaly And Mineral Prospectivity Mapping in GIS*. Elsevier.
- Hamilton, W., Ying, Z., Leskovec, J., 2017. Inductive representation learning on large graphs. *Advances in Neural Information Processing Systems*. Curran Associates, Inc.
- Hou, Z., Zhao, Z., Gao, Y., Yang, Z., Jiang, W., 2006. Tearing and dischronal subduction of the Indian continental slab: Evidence from Cenozoic Gangdese volcano-magmatic rocks in south Tibet. *Acta Petrol. Sin.* 22, 761–774.
- Ji, W.-Q., Wu, F.-Y., Liu, C.-Z., Chung, S.-L., 2012. Early Eocene crustal thickening in southern Tibet: New age and geochemical constraints from the Gangdese batholith. *J. Asian Earth Sci.* 53, 82–95.
- Kipf TN, Welling M. Semi-supervised classification with graph convolutional networks. arXiv Preprint arXiv:160902907 2016.
- Li G, Muller M, Thabet A, Ghanem B. DeepGCNs: Can GCNs Go As Deep As CNNs?, 2019, p. 9267–76.
- Li, L., Xie, C., Ren, Y., Yu, Y., Dong, Y., Gao, Z., et al., 2020a. Discovery of Late Triassic mineralization in the Gangdese Metallogenic Belt, Tibet: The Banduo Pb-Zn deposit, Somdo Area. *Ore Geol. Rev.* 126, 103754.
- Li, S., Chen, J., Xiang, J., 2020b. Applications of deep convolutional neural networks in prospecting prediction based on two-dimensional geological big data. *Neural Comput. Appl.* 32, 2037–2053.
- Li, T., Zuo, R., Xiong, Y., Peng, Y., 2021. Random-drop data augmentation of deep convolutional neural network for mineral prospectivity mapping. *Nat. Resour. Res.* 30, 27–38.
- Ma, L., Pal, S., Yitian, Z., Zhou, J., Yingxue, Z., Coates, M., 2024. CKGConv: general graph convolution with continuous kernels. In: *Proceedings of the 41st International Conference on Machine Learning*, pp. 33902–33924.
- Pan G, Ding J, Yao D, Wang L. Geological Map of the Tibetan Plateau and Adjacent Areas (1: 1,500,000) 2004.

- Pan, G., Wang, L., Li, R., Yuan, S., Ji, W., Yin, F., et al., 2012. Tectonic evolution of the Qinghai-Tibet plateau. *J. Asian Earth Sci.* 53, 3–14.
- Rajesh, H., 2004. Application of remote sensing and GIS in mineral resource mapping-An overview. *J. Mineral. Petrol. Sci.* 99, 83–103.
- Rodriguez-Galiano, V., Chica-Olmo, M., Chica-Rivas, M., 2014. Predictive modelling of gold potential with the integration of multisource information based on random forest: a case study on the Rodalquilar area, Southern Spain. *Int. J. Geogr. Inf. Sci.* 28, 1336–1354.
- Rubinstein, R., 1999. The Cross-Entropy Method for Combinatorial and Continuous Optimization. *Methodol. Comput. Appl. Probab.* 1, 127–190. <https://doi.org/10.1023/A:1010091220143>.
- Scarselli, F., Gori, M., Tsoi, A.C., Hagenbuchner, M., Monfardini, G., 2008. The graph neural network model. *IEEE Trans. Neural Netw.* 20, 61–80.
- Shepard, D., 1968. A two-dimensional interpolation function for irregularly-spaced data. In: Proceedings of the 1968 23rd ACM national conference. Association for Computing Machinery, New York, NY, USA, pp. 517–524. doi: 10.1145/800186.810616.
- Shi, L., Xu, Y., Zuo, R., 2024. A Heterogeneous Graph Construction Method for Mineral Prospectivity Mapping. *Nat. Resour. Res.* 1–12.
- Shihombing, F.M., Palin, R.M., Hughes, H.S., Robb, L.J., 2024. Improved mineral prospectivity mapping using graph neural networks. *Ore Geol. Rev.* 106215.
- Singer, D.A., 2021. How deep learning networks could be designed to locate mineral deposits. *J. Earth Sci.* 32, 288–292.
- Singer, D.A., Kouda, R., 1996. Application of a feedforward neural network in the search for Kuroko deposits in the Hokuroku district, Japan. *Math. Geol.* 28, 1017–1023.
- Talebi, H., Mueller, U., Peeters, L., Otto, A., De Caritat, P., Tolosana-Delgado, P., et al., 2022. Stochastic modelling of mineral exploration targets. *Math Geosci* 54, 593–621.
- Tang, J., Lang, X., Xie, F., Gao, Y., Li, Z., Huang, Y., et al., 2015. Geological characteristics and genesis of the Jurassic No. I porphyry Cu-Au deposit in the Xiongcuo district, Gangdese porphyry copper belt, Tibet. *Ore Geol. Rev.* 70, 438–456.
- Tang, J.-X., Liu, H.-F., Lang, X.-H., Zhang, J.-S., Zheng, W.-B., Ying, L.-J., 2012. Minerogenetic series of ore deposits in the east part of the Gangdese metallogenic belt. *Diqiu Xuebao (Acta Geoscientica Sinica)* 33, 393–410.
- Velickovic, P., Cucurull, G., Casanova, A., Romero, A., Lio, P., Bengio, Y., et al., 2017. Graph attention networks. *Stat* 1050, 10–48550.
- Wang, L., Liu, B., McKinley, J.M., Cooper, M.R., Li, C., Kong, Y., et al., 2021. Compositional data analysis of regional geochemical data in the Lhasa area of Tibet, China. *Appl. Geochem.* 135, 105108.
- Wang, L., Tang, J., Deng, J., Kang, H., Lin, X., Cheng, W., et al., 2015. The Longmala and Mengya's skarn Pb-Zn deposits, Gangdese region, Tibet: evidence from U-Pb and Re-Os geochronology for formation during early India-Asia collision. *Int. Geol. Rev.* 57, 1825–1842. <https://doi.org/10.1080/00206814.2015.1029540>.
- Wang, L., Tang, J., Zheng, W., Chen, W., Lin, X., Kang, H., et al., 2014. Study on metallogenesis of main molybdenum polymetallic deposits in the eastern section of the Gangdese metallogenic belt. *Geol. Rev.* 60, 363–379.
- Wu, Z., Pan, S., Chen, F., Long, G., Zhang, C., Philip, S.Y., 2020. A comprehensive survey on graph neural networks. *IEEE Trans. Neural Networks Learn. Syst.* 32, 4–24.
- Xie, M., Liu, B., Wang, L., Li, C., Kong, Y., Tang, R., 2023. Auto encoder generative adversarial networks-based mineral prospectivity mapping in Lhasa area, Tibet. *J. Geochem. Explorat.* 255, 107326.
- Xie, X., Wang, X., Zhang, Q., Zhou, G., Cheng, H., Liu, D., et al., 2008. Multi-scale geochemical mapping in China. *Geochem. Explor. Environ. Anal.* 8, 333–341.
- Xiong, Y., Zuo, R., Carranza, E.J.M., 2018. Mapping mineral prospectivity through big data analytics and a deep learning algorithm. *Ore Geol. Rev.* 102, 811–817.
- Xu, Y., Zuo, R., 2024. An interpretable graph attention network for mineral prospectivity mapping. *Math. Geosci.* 56, 169–190.
- Xu, Y., Zuo, R., Zhang, G., 2023. The graph attention network and its post-hoc explanation for recognizing mineralization-related geochemical anomalies. *Appl. Geochem.* 155, 105722.
- Xu, Z., Zheng, B., Wang, Q., 2021. From accretion to collision: situation and outlook. *Acta Geol. Sin.* 95, 75–97.
- Xuan-Xue, M., Guo-Chen, D., Zhi-Dan, Z., Su, Z., Liang-Liang, W., Rui-Zhao, Q., et al., 2005. Spatial and temporal distribution and characteristics of granitoids in the Gangdese, Tibet and implication for crustal growth and evolution. *Geol. J. China Univ.* 11, 281.
- Xuejing, X., Xuzhan, M., Tianxiang, R., 1997. Geochemical mapping in China. *J. Geochem. Explor.* 60, 99–113.
- Yang, N., Zhang, Z., Yang, J., Hong, Z., Shi, J., 2021. A convolutional neural network of GoogleNet applied in mineral prospectivity prediction based on multi-source geoinformation. *Nat. Resour. Res.* 30, 3905–3923.
- Zhou, J., Cui, G., Hu, S., Zhang, Z., Yang, C., Liu, Z., et al., 2020. Graph neural networks: A review of methods and applications. *AI Open* 1, 57–81.
- Zuo, R., 2020. Geodata science-based mineral prospectivity mapping: A review. *Nat. Resour. Res.* 29, 3415–3424.
- Zuo, R., Carranza, E.J.M., 2023. Machine learning-based mapping for mineral exploration. *Math. Geosci.* 55, 891–895.
- Zuo, R., Xu, Y., 2023. Graph deep learning model for mapping mineral prospectivity. *Math. Geosci.* 55, 1–21.